Jacob Seboly

Assessing Tornado Vulnerability in Tennessee through Tornado Incidence and Societal Exposure

Faculty Sponsor

Dr. Esra Ozdenerol

Abstract

Tornadoes are the deadliest type of natural disaster in Tennessee, and detailed analysis of tornado vulnerability in Tennessee is necessary to improve preparedness. This study defines tornado incidence as the likelihood of a particular location to experience tornadoes, and societal exposure as the ability of a particular community to cope with and recover from tornado disasters. Tornado incidence and societal exposure are combined to estimate overall tornado vulnerability across the state on a county-by-county basis. Tornado count data are used to assess tornado incidence. Regression analysis indicates that out of a selection of social vulnerability indices from previous literature, The Center for Disease Control and Prevention's SVI index best predicts tornado fatalities, so it is used to estimate societal exposure. The study found that tornado vulnerability generally decreases from southwest to northeast across the state with Hardeman, Haywood, Lake, and Lauderdale counties identified as most vulnerable.

Introduction

Tornadoes represent the deadliest category of natural disaster in Tennessee. From 1950 to 2017, tornadoes inflicted 347 deaths, 4,500 injuries, and $1.8 billion in property damage in Tennessee (NCEI, 2019). These statistics indicate that there is much room for improvement for tornado preparedness in Tennessee. A detailed assessment of tornado vulnerability on a county-by-county basis across Tennessee will likely be a valuable tool for decision-makers who seek to improve preparedness in the state.

This study uses a conceptual model adapted from Dixon and Moore (2012) which defines tornado vulnerability as a function of climatological conditions (tornado incidence) and socioeconomic conditions (societal exposure). Tornado incidence represents the frequency and strength of tornadoes affecting a particular community. It will be calculated using data on the geographic location and Fujita Scale rating of historical tornadoes. Societal exposure represents the ability of a particular community to cope with and recover from natural disasters including tornadoes (Flanagan, Hallisey, Adams, & Lavery, 2018). It will be assessed through the calculation of various social vulnerability indices. These indices incorporate socioeconomic variables such as income, education, and demographics and calculate a single value which represents the social vulnerability of a given location. Two social vulnerability indices have been designed for use with natural disasters (Flanagan et al., 2018), (Cutter, Boruff, & Shirley, 2003), but their effectiveness in predicting tornado impacts specifically has not been assessed. This study will provide a basic assessment of these two indices and their effectiveness in predicting tornado fatalities with the more effective index chosen to estimate societal exposure for this study.

Previous tornado studies in Tennessee have been performed; however, those studies focused on tornado incidence only (Brown, Ellis, & Bleakney, 2016), (Ozdenerol, 2004). The authors agreed that tornadoes are generally most common on the western side of the Tennessee and least common on the eastern side. However, it is important to also ascertain where the highest societal exposure to tornadoes lies. This study will build upon the previous studies by combining both tornado incidence and societal exposure to form a more well-rounded picture of tornado vulnerability in Tennessee.

Literature Review

Tornado Incidence in Tennessee

While Tennessee is not part of the traditional "Tornado Alley", it is, according to recent research, one of the most tornado-prone states in the nation.

Notably, western Tennessee has suffered the highest rate of tornado-related fatalities in the United States since 1880 (Ashley, 2007). This region, along with much of the Southeast, is often referred to as "Dixie Alley" and is known for fast-moving tornadoes, nocturnal tornadoes, and tornadoes with high fatality rates (Ashley, 2007). Spatial analysis using kernel density estimation indicates that the area of highest tornado risk in the United States is not limited to traditional Tornado Alley but rather "extends roughly from Oklahoma to Tennessee and northwestern Georgia" (Coleman & Dixon, 2014, p. 366). Since this corridor encompasses western and middle Tennessee, these areas can be characterized as highly tornado-prone. Dixon et al. (2011) also noted that "Tornado Alley" should be extended to incorporate the southeastern United States including Tennessee. Also noteworthy is that Tennessee's tornado count in its peak years eclipses that of the Plains states (Brown et al., 2016).

Additionally, the observed effect of climate change on the spatial distribution of tornadoes indicates that tornado risk in Tennessee may increase in the future. The Southeast, including Tennessee, experienced an increase in tornadic activity between 1984-2013 compared with 1950-1983 (Agee et al., 2016) Regression analysis also indicated a statistically significant upward trend in Southeast tornado counts (Moore, 2018). STP (Significant Tornado Parameter) values in the Southeast also demonstrated a statistically significant increase since 1979 (Gensini & Brooks, 2018). In all three of these studies, Tennessee was included within the Southeast region suggesting that the frequency of tornadoes in Tennessee is increasing. Since Tennessee is already one of the most tornado-prone states in the nation in terms of tornado counts and fatality counts, and tornado risk is expected to increase in the future, it is possible that Tennessee will become an epicenter for tornadic activity later in the 21st century and beyond.

Societal Exposure in Tennessee

Disproportionately high tornado fatality rates in Tennessee suggest that the state suffers significant societal exposure to tornadoes. From 1880 to 2007, an area of southwestern Tennessee near Memphis suffered the highest tornado fatality rate in the nation (Ashley, 2007). Several explanations for this high fatality rate have been proposed including high frequencies of nocturnal tornadoes (Brown et al., 2016) and off-season tornadoes (Brooks, Doswell, & Kay, 2003), the prevalence of mobile homes (Sutter & Simmons, 2010), and a lack of awareness and preparedness among residents (Ellis et al., 2018). Nocturnal tornadoes pose a greater threat to human life because they are difficult to see and because they strike while most of the population is asleep and unable to receive tornado warnings (Ashley, Krmenec, & Schwantes,

2008). Fall and winter tornadoes are more dangerous because daylight is shorter during these seasons leading to more nocturnal tornadoes (Ashley et al., 2008) and because residents are less likely to be mentally aware of tornado risk (Brown et al., 2016). The danger that tornadoes pose to mobile homes is well documented. An individual is 10 to 20 times more likely to die from the same tornado in a mobile home than in a permanent home (Brooks & Doswell, 2001), (Simmons & Sutter, 2006). These factors, which have combined to produce Tennessee's high fatality rate, exemplify the state's high societal exposure to tornadoes. Tennessee's increasing tornado incidence rate and significant societal exposure to tornadoes underscore the importance of assessing tornado vulnerability patterns and improving preparedness throughout the state.

Methodology

Study Area

Tornado vulnerability was assessed on a county-by-county basis throughout Tennessee. Additionally, in order to make this study more useful for National Weather Service (NWS) operations, the study area was expanded to include additional counties from neighboring states such that the entirety of the NWS Memphis, Nashville, Morristown, and Huntsville forecast areas are covered. This resulted in the addition of ten Alabama counties, eleven Arkansas counties, twenty-two Mississippi counties, two Missouri counties, two North Carolina counties, and seven Virginia counties.

Tornado Incidence Data and Analysis

Tornado path data representing all reported tornadoes between 1950 and 2017 were obtained from the Storm Prediction Center. These data were used to determine tornado counts and incidence. F0/EF0 and F1/EF1 tornadoes were excluded because of reporting bias in urban areas (Anderson, Wikle, Zhou, & Royle, 2007). Weighted tornado counts were calculated according to the following scheme: F2/EF2 = 2 points, F3/EF3 = 3 points, F4/EF4 = 4 points, F5/EF5 = 5 points. This weighting scheme is adapted from the Texas study (Dixon & Moore, 2012). The distribution of tornado reports at the county level was noisy. Since the sample size of tornado events is rather small (less than 40 tornadoes per county), county-level tornado counts are likely influenced more by chance than by underlying tornado risk. To eliminate this issue, tornado incidence for each county was estimated using the tornado count within 50 miles of the county's centroid. This process increased the sample size for each county, resulting in a much smoother spatial distribution of tornado incidence.

Tornado fatality, injury, and property damage data were obtained from the NCEI Storm Events Database. The SPC tornado database has data for each tornado, but it is not divided on a county-by-county basis. Thus, the NCEI data was necessary to determine fatality, injury, and property damage totals per county.

Societal Exposure Data and Analysis

Societal exposure was estimated in this study through social vulnerability indices. Calculating a social vulnerability index is a well-established method of identifying which counties are best prepared to cope with and recover from a potential natural disaster. Two social vulnerability indices are relevant for the purposes of this study: the SVI and the SoVI. The SVI was designed by the Centers for Disease Control and Prevention (CDC) (Flanagan et al., 2018). It utilizes fifteen socioeconomic variables: per capita income, poverty, unemployment, education level, population age 65 or older, population age 17 or younger, disabled population, single-parent households, minority population, non-English-speaking population, multi-unit structures, mobile homes, crowded households, households with no vehicle, and population in group quarters (Flanagan et al., 2018). SVI values are calculated by summing the national percentile values of each of the fifteen variables for each respective county. Thus, the lowest possible score is 0 and the highest possible score is 15. In practice, the lowest values are generally around 6 while the highest values are around 12. Higher values signify greater vulnerability to disasters (Flanagan et al., 2018). The SoVI was originally designed by Susan L. Cutter, Bryan J. Boruff, & W. Lynn Shirley in 2003, with further updates following. This study utilizes the SoVI 2010-14, which is calculated using 29 variables. An additive model is used to combine the variables and the result is normalized, producing a Z-score. Negative values represent lesser vulnerability to disasters while positive values represent greater vulnerability (Cutter et al., 2003). These two indices were then evaluated based on their effectiveness in predicting tornado fatalities.

The SVI and SoVI indices were compared using regression modeling to estimate which index exhibits stronger correlation with tornado fatalities. A general empirical validation for these indices, accounting for all natural disaster types, had been performed by Bakkensen, Fox-Lent, Read, and Linkov (2017). The dataset for this study included all natural disasters in the Southeastern U.S. from 2000-2012. The results indicated that the SVI is a statistically significant predictor of disaster-related property damage and fatalities while the SoVI is a statistically significant predictor of property damage but not fatalities. Based on these results, it was hypothesized that the SVI would perform better, since, in the Bakkensen et al. study, it exhibited

statistically significant correlation with fatality counts while the SoVI did not.

A dataset of fatal tornado events was compiled using data from the NCEI Storm Events Database. All tornadoes within the study area between 1950 and 2017 which caused at least one fatality were selected. The resulting dataset contained 204 fatal tornado events. The NCEI Database provides tornado data on an event-by-event basis. Therefore, if multiple fatal tornadoes occurred in the same county on the same day, a separate entry is provided for each tornado. The date, time, county, population density of the county in the closest census, fatality count, and Fujita Scale rating of each fatal tornado event were recorded. Population density was determined by rounding the tornado year to the nearest decade and using the appropriate census. For example, a 1954 tornado would be paired with 1950 Census data while a 1955 tornado would be paired with 1960 Census data. All other storm-related data were obtained from the Storm Events Database. The 2014 SVI and 2010-2014 SoVI values for the appropriate county were also included in each tornado's entry. These data were obtained at the county level from the authors' websites. To estimate population density, census data from 1950-2010 at the county level were obtained from the National Historical GIS.

For this study, the negative binomial regression model from Bakkensen et al. (2017) was adapted with slight modifications. Negative binomial regression is the appropriate model for this type of analysis because fatalities represent count data and because fatality data is overdispersed (the variance is greater than the mean) and extremely right skewed. Underlying risk rate was omitted because that variable was mainly useful for dealing with a wide range of disasters over a large study area. Tornado Fujita rating was added to the model because it is an extremely significant factor in determining a tornado's impact. Thus, the explanatory variables used in this study are population density, tornado strength, and social vulnerability, represented by the SVI and SoVI. Values for the SVI and SoVI were both normalized. These modifications were necessary because the Bakkensen model incorporated all disaster types while this study incorporates only tornadoes.

The model equation was designed as follows:

$$F_{i,j,t} = \beta_0 + B_1 I_i + B_2 \, ln(P_{i,t}) + B_3 F_j + \mu_{i,j,t}$$

$F_{i,j,t}$ represents fatality count of tornado j in county i in year t. I_i represents social vulnerability in county i. The normalized SVI and SoVI were used in this term. $P_{i,t}$ represents population density in county i in year t,

in population per square mile. F_j represents the Fujita Scale rating of tornado j. $\mu_{i,j,t}$ represents the error term.

The model was run twice; once with the SVI as an explanatory variable and once with the SoVI as an explanatory variable. The correlation between social vulnerability index values and fatalities was noted for each run. Since the indices were both normalized, their coefficients (β_1) could also be compared. Several additional sensitivity tests were also performed. The model was run with 2014 population density (at the census tract level) replacing historical population density. This insured that the model was not significantly affected by tornadoes which passed through dense population centers. Census tract population estimates for 2014 were acquired from the Centers for Disease Control and Prevention. Finally, the model was also run with casualty counts (fatalities + injuries) replacing fatality counts to see if the results could also be applied to casualty counts.

The results of the regression models with respect to the SVI and SoVI, with the addition of several sensitivity tests, are displayed in the following tables.

Variable	Coefficient	Std. Error	Z-Score	Significant (p<0.05)?
SVI	0.14081	0.06143	0.011	Yes
Fujita Rating	0.61778	0.05833	<0.001	Yes
Population	0.13788	0.07513	0.033	Yes

Table 1. SVI vs. Fatalities Regression Model Results

Variable	Coefficient	Std. Error	Z-Score	Significant (p<0.05)?
SoVI	0.08182	0.06122	0.091	No
Fujita Rating	0.60955	0.05958	<0.001	Yes
Population	0.11092	0.07582	0.071	No

Table 2. SoVI vs. Fatalities Regression Model Results

Variable	Significant (p<0.05)? Historical Population	Significant (p<0.05)? 2014 Population	Significant (p<0.05)? Casualties
SVI	Yes	Yes	No
SoVI	No	No	No

Table 3. Sensitivity Tests

The SVI exhibited a statistically significant positive correlation with fatality counts, while the SoVI did not. The SVI's coefficient was also higher, meaning that a one-point increase in the SVI corresponded to more fatalities than a one-point increase in the SoVI. When 2014 tract-level population density was substituted for historical county-level population density, the results did not change. The SVI had a statistically significant positive correlation with fatality counts, while the SoVI did not. Neither index had a statistically significant correlation with casualty counts. Because only the SVI had a statistically significant correlation with tornado fatalities, it was chosen for use in the societal exposure and tornado vulnerability calculations.

Tornado Vulnerability Calculations

This study used the same three calculation methods as Dixon & Moore (2012) to incorporate both tornado incidence and societal exposure into an overall

tornado vulnerability index. The CDC's Social Vulnerability Index (SVI) was used as the input variable for societal exposure since it outperformed the SoVI in predicting tornado fatalities. For each county, the tornado count (weighted, see section 3.2 for calculation) within 50 miles will be used as the input variable for tornado incidence. Percentiles and Z-scores for tornado incidence and societal exposure were calculated for each county.

Method 1 was designed to most effectively convey the unique combination of societal exposure and tornado incidence that each county experiences. For Method 1, the two input variables (societal exposure, tornado incidence) were not combined but instead classified separately. Each variable was categorized for each county as low (Z-score less than -1.00), moderate ($-1.00 < Z < +1.00$), or high ($Z > +1.00$). Since Method 1 preserves the distinction between societal exposure and tornado incidence, it is a useful tool for assessing the specific details of each county's situation. While a county with high tornado incidence and low societal exposure might be classified similarly to a county with low tornado incidence and high societal exposure by Methods 2 and 3, Method 1 preserves a distinction between the two counties.

Method 2 was designed to provide a balanced view of the combined effects of tornado incidence and societal exposure. For Method 2, the Z-scores of tornado incidence and societal exposure were added for each respective county. Method 2 is somewhat susceptible to statistical outliers and tends to emphasize counties with high societal exposure even if tornado incidence is low or nonexistent (Dixon & Moore, 2012).

Method 3 was designed to highlight the counties with high scores in both tornado incidence and societal exposure and minimize the impact of statistical outliers. Method 3 scores were calculated by multiplying the percentile scores of tornado incidence and societal exposure, resulting in a value between 0 (lowest) and 1 (highest). For Method 3, most counties receive scores close to 0, while the few counties with high values in both variables score closer to 1.

Results

Counties were classified according to their z-score of tornado vulnerability according to the following scheme: very low ($z < -1.50$), low ($-1.50 < z < -0.50$), moderate ($-0.50 < z < +0.50$), high ($+0.50 < z < +1.50$), and very high ($z > +1.50$). According to the calculations from Method 1 (see Figure 4), the highest tornado incidence is concentrated in north Alabama. Arkansas, Mississippi, and western and middle Tennessee were classified as experiencing moderate tornado incidence. East Tennessee and the Appalachian region enjoy the lowest tornado incidence. The highest values of societal

exposure are concentrated within the Mississippi River Delta, but there are also high societal exposure values in a few scattered counties outside the Delta. Poinsett County, Arkansas and Franklin County, Alabama were the only counties classified as "high" in both variables. Knox, Blount, and Washington Counties, in Tennessee and Washington County, Virginia were classified as "low" in both variables.

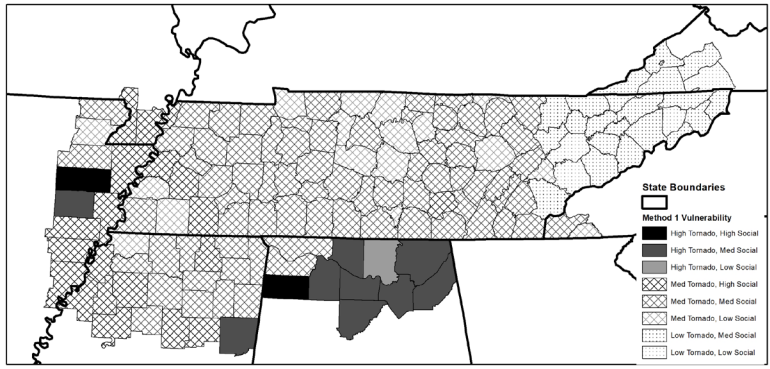

Figure 4. Method 1 Tornado Vulnerability

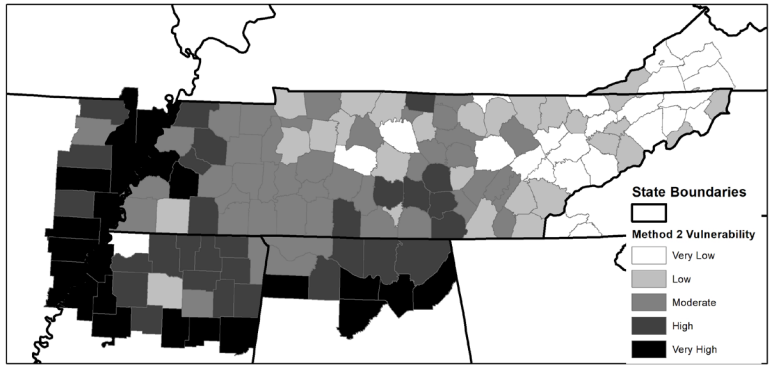

Figure 5. Method 2 Tornado Vulnerability

According to Method 2 (see Figure 5), the most tornado-vulnerable areas are along the southern and western periphery of the study area. Specifically, this area includes the Eastern Arkansas counties, the Mississippi Delta counties, and the counties in northern Mississippi and Alabama which comprise the southern edge of the study area. The Arkansas counties appear to be rated as vulnerable because of social factors, while the Mississippi and Alabama counties are rated as vulnerable because of their high tornado incidence. The county with the highest Method 2 vulnerability score is Marshall County, Alabama (+3.61). The least vulnerable area according to Method 2 is eastern Tennessee where tornadoes are comparatively rare. Societal exposure is also generally low in this area. The county with the lowest Method 2 vulnerability score is Williamson County, Tennessee (-3.47). Method 2 vulnerability scores for all counties in the study area are provided in Appendix A, Tables 4 and 5.

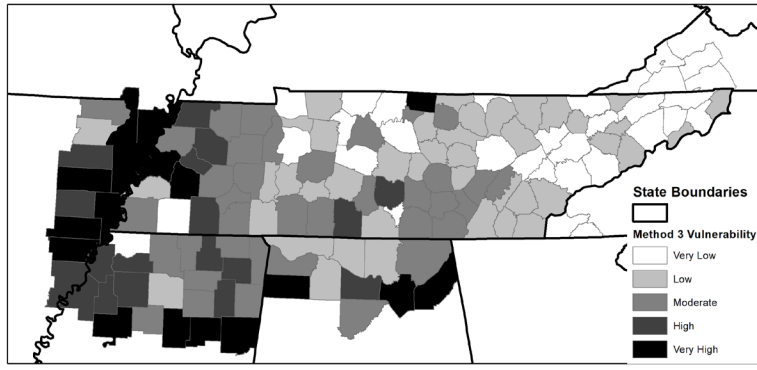

Figure 6. Method 3 Tornado Vulnerability

The southern and western periphery of the study area were also identified as the most tornado-vulnerable areas by Method 3 (Figure 6). However, Method 3 is designed to point out individual counties with high vulnerability in both variables rather than general areas. According to Method 3, the most vulnerable counties are Mississippi and Poinsett, AR; Dunklin, MO; Lake and Lauderdale, TN; Chickasaw, MS; and Franklin and Marshall, AL. Dunklin County, Missouri received the highest Method 3 vulnerability score (0.856). Williamson County, Tennessee and Russell County, Virginia tied for the lowest Method 3 vulnerability score (0.0).

DISCUSSION

SVI Comparison Implications

According to regression analysis on the two social vulnerability indices, the SVI was a more effective predictor of tornado fatalities in Tennessee than the SoVI. However, this result would not necessarily be applicable to other regions of the United States. Socioeconomic patterns and tornado seasonality patterns vary across the United States, so it is possible that the SoVI might outperform the SVI in other regions of the country. Further investigation is needed on this topic.

Fatalities and casualties were the only dependent variables modeled in this study. While the SVI predicted fatalities more effectively than the SoVI, there was no significant difference between the indices in predicting casualties. Therefore, no assumptions should be made about the correlation of the SVI and SoVI with other disaster impact variables such as property damage. Finally, the findings of this study should not be applied to vulnerability studies for other types of natural disasters. It is feasible that the SoVI would predict fatality counts for other types of disasters better than the SVI.

Possible Further Research

As mentioned in the literature review, the study of tornado vulnerability as a function of both tornado incidence and societal exposure is an undeveloped field of research. Currently, social vulnerability to tornadoes has only been assessed in Oklahoma, Texas, and Tennessee. Tornado vulnerability assessments which include socioeconomic variables need to be performed for the rest of the nation especially in the Great Plains, Midwest, and Southeast where tornado incidence is highest. The three methods used in this study and in Dixon & Moore (2012) to combine tornado incidence and societal exposure also must be tested, compared, and validated. Additional methods could also be proposed and validated.

This study included a basic assessment of the effectiveness of two social vulnerability indices, the SVI and SoVI, in predicting tornado fatalities. More widespread assessments of these indices are needed. It also remains unclear which index better predicts casualties and property damage. Further development of place-based weighted indices of social vulnerability would prove useful in this field as well.

Conclusion

This study assessed tornado vulnerability as a function of tornado incidence and societal exposure over an area including all of Tennessee and a selection

of counties from neighboring states. This area was designed to include all counties under the responsibility of the Memphis, Nashville, Huntsville, and Morristown offices of the National Weather Service.

The highest tornado incidence in the study area is concentrated in northern Alabama. Northern Mississippi, eastern Arkansas, and western Tennessee suffer moderate to high tornado incidence. Eastern Tennessee and southwestern Virginia have the lowest tornado incidence. Societal exposure is distributed more widely throughout the area, but notable regions included the Mississippi River Delta and isolated counties in Alabama, Mississippi, and Tennessee. The most tornado-vulnerable areas were identified to be northern Alabama, northern Mississippi, eastern Arkansas, and western Tennessee. The least vulnerable areas are eastern Tennessee and southwestern Virginia. Similar tornado vulnerability assessments are still needed across many areas of the United States.

Two social vulnerability indices, the SVI and SoVI, were compared for their effectiveness in predicting tornado fatalities within the study area. A negative binomial regression model was prepared with fatalities as the independent variable and population, social vulnerability, and tornado magnitude as the dependent variables. The SVI exhibited a statistically significant correlation with tornado fatalities while the SoVI did not. Further research on the appropriate use of social vulnerability indices in assessing tornado vulnerability is needed.

References

Agee, E., Larson, J., Childs, S., & Marmo, A. (2016). Spatial Redistribution of U.S. Tornado Activity between 1954 and 2013. *Journal of Applied Meteorology & Climatology*, *55*(8), 1681–1697. https://doi.org/10.1175/JAMC-D-15-0342.1

Anderson, C. J., Wikle, C. K., Zhou, Q., & Royle, J. A. (2007). Population Influences on Tornado Reports in the United States. *Weather and Forecasting*, *22*(3), 571–579. https://doi.org/10.1175/WAF997.1

Ashley, W. S. (2007). Spatial and Temporal Analysis of Tornado Fatalities in the United States: 1880–2005. *Weather and Forecasting*, *22*(6), 1214–1228. https://doi.org/10.1175/2007WAF2007004.1

Ashley, W. S., Krmenec, A. J., & Schwantes, R. (2008). Vulnerability due to Nocturnal Tornadoes. *Weather and Forecasting*, *23*(5), 795–807. https://doi.org/10.1175/2008WAF2222132.1

Bakkensen, L. A., Fox-Lent, C., Read, L. K., & Linkov, I. (2017). Validating Resilience and Vulnerability Indices in the Context of Natural Disasters. *Risk Analysis*, *37*(5), 982–1004. https://doi.org/10.1111/risa.12677

Brooks, H. E., Doswell, C. A., & Kay, M. P. (2003). Climatological Estimates of Local Daily Tornado Probability for the United States. *Weather & Forecasting*, *18*(4), 626–640. https://doi.org/10.1175/1520-0434(2003)018<0626:CEOLDT>2.0.CO;2

Brooks, H. E., & Doswell III, C. A. (2001). Normalized Damage from Major Tornadoes in the United States: 1890-1999. *Weather & Forecasting*, *16*(1), 168. https://doi.org/10.1175/1520-0434(2001)016<0168:NDFMTI>2.0.CO;2

Brown, V. M., Ellis, K. N., & Bleakney, S. A. (2016). Tennessee Tornado Climate. *Southeastern Geographer*, *56*(1), 118–133. https://doi.org/10.1353/sgo.2016.0008

Coleman, T. A., & Dixon, P. G. (2014). An Objective Analysis of Tornado Risk in the United States. *Weather & Forecasting*, *29*(2), 366–376. https://doi.org/10.1175/WAF-D-13-00057.1

Cutter, S. L., Boruff, B. J., & Shirley, W. L. (2003). Social Vulnerability to Environmental Hazards. *Social Science Quarterly*, *84*(2), 242.

Dixon, D. P., Mercer, A. E., Choi, J., & Allen, J. S. (2011). TORNADO RISK ANALYSIS: Is Dixie Alley an Extension of Tornado Alley? *Bulletin of the American Meteorological Society*, *92*(4), 433.

Dixon, R. W., & Moore, T. W. (2012). Tornado Vulnerability in Texas. *Weather, Climate, and Society*, *4*(1), 59–68. https://doi.org/10.1175/WCAS-D-11-00004.1

Ellis, K. N., Mason, L. R., Gassert, K. N., Elsner, J. B., & Fricker, T. (2018). Public perception of climatological tornado risk in Tennessee, USA. *International Journal Of Biometeorology*, *62*(9), 1557–1566. https://doi.org/10.1007/s00484-018-1547-x

Flanagan, B. E., Hallisey, E. J., Adams, E., & Lavery, A. (2018). Measuring Community Vulnerability to Natural and Anthropogenic Hazards: The Centers for Disease Control and Prevention's Social Vulnerability Index. *Journal of Environmental Health*, (10), 34.

Gensini, V. A., & Brooks, H. E. (2018). Spatial trends in United States tornado frequency. *Npj Climate and Atmospheric Science*, (1), 1. https://doi.org/10.1038/s41612-018-0048-2

Hout, E. M., Yuan, M., McIntosh, J., & Weaver, C. (2010). *Spatial Analysis of Tornado Vulnerability Trends in Oklahoma and Northern Texas*. Presented at the 25th Conference on Severe and Local Storms, Denver, CO.

Moore, T. W. (2018). Annual and seasonal tornado trends in the contiguous United States and its regions. *International Journal of Climatology*, (3), 1582. https://doi.org/10.1002/joc.5285

National Centers for Environmental Information. (2019, May). NCEI Storm Events Database. NCEI Storm Events Database. https://www.ncdc.noaa.gov/stormevents/

Ozdenerol, E. (2004). *Tornado Hazards in Tennessee: Understanding Vulnerability to Tornadoes in Tennessee*.

Simmons, K. M., & Sutter, D. (2006). Direct Estimation of the Cost Effectiveness of Tornado Shelters. *Risk Analysis: An International Journal*, *26*(4), 945–954. https://doi.org/10.1111/j.1539-6924.2006.00790.x

Sutter, D., & Simmons, K. M. (2010). Tornado fatalities and mobile homes in the United States. *Natural Hazards*, (1), 125. https://doi.org/10.1007/s11069-009-9416-x

Jeremy Walker graduated in spring 2020 from Weber State University. He earned his degree *magna cum laude* with departmental honors in physics. In the summer of 2019, he conducted research at the University of Memphis in the Research Experience for Undergraduates program funded by the National Science Foundation. Jeremy has done two research projects in computational physics and presented one project at the American Physical Society's Four Corners meeting in 2018. He has been accepted to a master's program in applied physics at the University of Oregon.

Jeremy Walker

A Molecular Dynamics Study of Lipid Membranes Cushioned by Polymer Brushes

Faculty Sponsor

Dr. Mohammed Lardji

Abstract

We present a numerical study of self-assembled lipid membranes, that are cushioned by polymer brushes, using molecular dynamics simulations of a coarse-grained implicit solvent model.

Introduction

Lipid bilayers are a crucial component of life. When a group of lipids is exposed to water, the hydrophobic groups turn toward each other while the hydrophilic groups turn toward the water. These bilayers make up the ever-important lipid membrane of cells. The lipid membrane acts as a barrier between the inner and outer parts of the cell, provides structural integrity for the cell, and supports numerous large transmembrane proteins needed for proper cellular function. Without lipid membranes, cells would spill out of their bounds and not even simple single celled organisms could survive.

Prior studies have employed a variety of techniques to study the function, structure, and dynamics of lipid bilayers. At the most basic level, substrate supported studies can be done (McCabe, 2013; Andersson, 2016; Deverall, 2005). In these experiments, the membrane is placed directly on a substrate with a water layer cushion that is a few nanometers thick. This limits the motion of the membrane in the direction perpendicular to the substrate and is an especially poor way to study transmembrane proteins because they are too large and often denature with excessive contact with the substrate due to their protrusion below the bilayer (McCabe, 2013). To overcome these obstacles, an additional layer of polymer can be added below the membrane to act as a cushion. This polymer supported model allows transmembrane proteins to sink into the polymer and as such, they are less likely to denature. One type of polymer support is a polymer brush, which is formed by chemically tethering polymer chains to a substrate and introducing a membrane on the free ends. In this computational study, we will simulate a polymer brush support because it mimics the cytoskeleton of the cell and as such, is a better model to study biological processes. We aim to study the mutual effects of the membrane and the polymer brush interactions and to increase the theoretical understanding of this model for use in future experiments.

Model And Computational Method

A coarse-grained implicit-solvent model was used (Revalee, 2008; Laraji, 2016), in which a lipid molecule is coarse-grained into a semi-flexible chain composed of one head (h) bead and two tail (t) beads. The potential energy of the lipid bilayer has three contributions:

$$U(\{r_i\}) = \sum U_0^{\alpha_i \alpha_j}(r_{ij}) + \sum_{(i,j)} U_{bond}(r_{ij}) + \sum_{(i,j,k)} U_{bend}(\vec{r}_i, \vec{r}_j, \vec{r}_k), \quad (1)$$

where $\vec{r}_i$ describes the coordinates of bead i, $r_{ij} = |\vec{r}_i - \vec{r}_j|$, and $\alpha_i (= h \text{ or } t)$ is the type of bead i. In Eq. (1), $U_0^{\alpha\beta}$ is a soft two-body potential, between beads of types α and β and separated by a distance r, and is a piece-wise function given by (Laradji, 2016),

$$U_0^{\alpha\beta}(r) = \begin{cases} (U_{max}^{\alpha\beta} - U_{min}^{\alpha\beta}) \dfrac{(r_m - r)^2}{r_m^2} + U_{min}^{\alpha\beta} & \text{if } r \le r_m \\ -2U_{min}^{\alpha\beta} \dfrac{(r_c - r)^3}{(r_c - r_m)^3} + 3U_{min}^{\alpha\beta} \dfrac{(r_c - r)^2}{(r_c - r_m)^3} & \text{if } r < r \le r_c \\ 0 & \text{if } r > r_c, \end{cases} \quad (2)$$

where $U_{max}^{\alpha\beta} > 0$ and $U_{min}^{\alpha\beta} \le 0$ for any pair (α, β). $U_{min}^{\alpha\beta} = 0$ implies a fully repulsive interaction between beads α and β, and $U_{min}^{\alpha\beta} < 0$ implies a short-range attraction between the two beads. The self-assembly of the lipids into thermodynamically stable bilayers is ensured by choosing $U_{min}^{hh} = U_{min}^{ht} = 0$ and a sufficiently negative value of U_{min}^{tt} (Laradji, 2016).

In Eq. (1), U_{bond} ensures connectivity between beads that belong to the same lipid chain and is given by

$$U_{\text{bond}}(r) = \frac{k_{\text{bond}}}{2}(r - a_b)^2, \quad (3)$$

where k_{bond} is the bond stiness coefficient and a_b is the preferred bond length. Finally, U_{bend} in Eq. (1) is a three-body potential that provides bending stiness to the lipid chains and is given by

$$U_{\text{bend}}(\vec{r}_{i-1}, \vec{r}_i, \vec{r}_{i+1}) = \frac{k_{\text{bend}}}{2} \left(\cos\varphi_0 - \frac{\vec{r}_{i,i-1} \cdot \vec{r}_{i,i+1}}{r_{i,i-1}\, r_{i,i+1}} \right)^2 \quad (4)$$

where k_{bend} is the bending stiness coefficient and φ_0 is the preferred splay angle of the lipid chain, taken to be 180°.

All beads are moved using a molecular dynamics scheme with a Langevin thermostat (Grest, 1986),

$$\dot{\vec{r}}_i(t) = \vec{v}_i(t) \tag{5}$$

$$m_i \dot{\vec{v}}_i(t) = -\nabla_i U(\{\vec{r}_i\}) - \Gamma \vec{v}_i(t) + \sigma \vec{\Xi}_i(t), \tag{6}$$

where m_i is the mass of bead i and Γ is a bead's friction coefficient. $\sigma\vec{\Xi}_i(t)$ is a random force with zero mean, and is uncorrelated for dierent particles, dierent times, and dierent components. Γ and σ are inter-related through the fluctuation-dissipation theorem leading to $\Gamma = \sigma^2 = 2k_BT$.

The simulations are performed in the *NVT* ensemble, where N is the total number of beads in the system. The model interaction parameters are given by,

$$\begin{aligned}
U^{hh}_{max} &= U^{ht}_{max} = 100\epsilon, \\
U^{tt}_{max} &= 200\epsilon, \\
U^{hh}_{min} &= U^{ht}_{min} = 0, \\
U^{tt}_{min} &= -6\epsilon, \\
U^{mm}_{max} &= xyz, \\
U^{mm}_{min} &= 0, \\
U^{mh}_{max} &= 1210\epsilon / r_m^2, \\
U^{mt}_{min} &= 0, \\
U^{mh}_{min} &= -\mathcal{E}, \\
^{k}bond &= 100\epsilon / r_m^2, \\
^{k}bend &= 100\epsilon, \\
r_c &= 2r_m, \\
a_b &= 0.7r_m.
\end{aligned} \tag{7}$$

In Eq. (7), $\mathcal{E}$ is the adhesion energy of a lipid head group per unit of area of the NP, and is henceforth used to define the *adhesion strength*.

All simulations are performed at $k_BT = 3.0\epsilon$, with a time step $\Delta t = 0.02\tau$, where $\tau = r_m (m/\epsilon)^{1/2}$. Eqs. (5) and (6) are integrated using the velocity-Verlet algorithm.

The bending modulus of the bare bilayer, with the interaction parameters given by Eq. (7), as extracted from the spectrum of the LM height fluctuations, is $\kappa \approx 30 k_BT$ (Laradji, 2016), which is comparable to that of DPPC in the fluid phase (Nagle, 2015). The length scale, r_m, is estimated from comparing the value of the thickness of the LM ~ $5r_m$, typical to phospholipid bilayer. We therefore estimate $r_m \approx 1$ nm. Hence, in the remainder of this article, all lengths are expressed in nanometers, and the adhesion strength, $\mathcal{E}$, is expressed in k_BT/nm^2.

Results

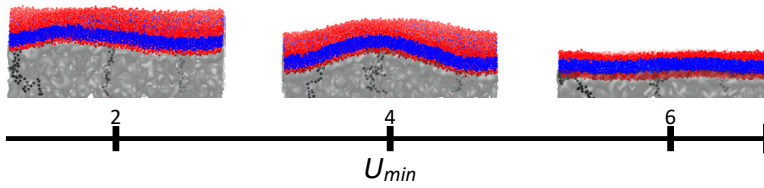

Figure 1. Typical configurations of the membrane for increasing $\mathcal{E}$. This system has a chain length N = 50, and a polymer brush grafting density σ = 0.1. Clearly, as $\mathcal{E}$ is increased, the average height of both the membrane and the polymer brush decrease. Note that between $\mathcal{E}$ = 2 and $\mathcal{E}$ = 4, the membrane fluctuations increased. The opposite occurred for $\mathcal{E}$ values past 4. Individual polymer chains have been highlighted to show how a typical chain behaves in the brush.

As shown in Fig. 1, the average height of the membrane and polymer brush decreases with increasing $\mathcal{E}$. Because of this compression, the density of the polymer layer is expected to increase. When a density profile is taken along the z-axis, the density of the polymer brush does indeed increase. However, this increase is largely localized near the membrane while the lower levels of the brush remain unchanged, as shown in Fig. 2. From this we conclude that a relatively highly dense layer of monomers forms directly under the bilayer. The increase in $\mathcal{E}$ favors an increase in the amount of contact between the lipid head groups and the monomers, which can only be achieved by

having the membrane move closer to the substrate.

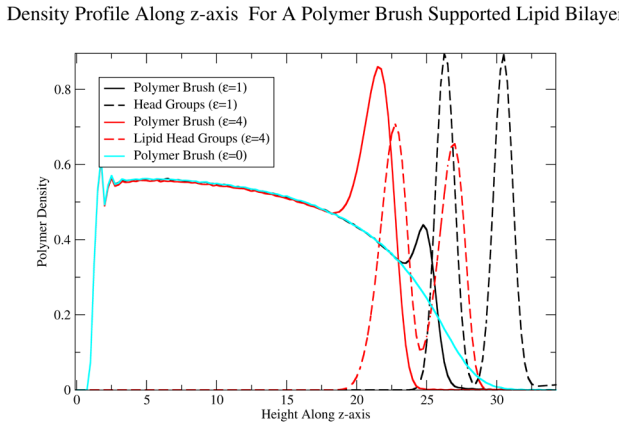

Figure 2. The density of the polymer brush is changed in the presence of a membrane. $\mathcal{E} = 0$ corresponds to a polymer brush that does not interact attractively with a membrane. With attraction to the lipid heads in the membrane, the polymer brush density increases near the lipid heads. However, the density of the lower levels is relatively unchanged. Additionally, the shortening and widening of the peaks associated with the lipid head groups when $\mathcal{E} = 4$ again imply the fluctuations of the membrane have increased as seen in Fig. 1. This data was collected from a system with $N = 50$ and $\sigma = 0.25$

Next, the bilayer's structure can first be characterized by the width of its fluctuations, $w = \sqrt{h^2 - (\bar{h})^2}$ where we define h as the height (z-coordinate) of a lipid head group in the top leaflet of the membrane. Fig. 3 and 4 demonstrate changes in the structure of the membrane caused by varying the grafting density or length of the polymer chains. There are three main features in Figs. 3 and 4. Namely, for very low $\mathcal{E}$, the membrane is not absorbed; followed by an abrupt decay in w at the absorption transition. For intermediate values of $\mathcal{E}$, there is an increase in the width, w. It then reaches a peak and then decreases for even higher $\mathcal{E}$. Because we expected a monotonic decrease in the fluctuations in the membrane, the intermediate increase of w vs. $\mathcal{E}$ is puzzling and needs further investigation. In contrast, the decrease of w vs. $\mathcal{E}$ for high $\mathcal{E}$ is expected. The non-monotonous behavior of w vs. $\mathcal{E}$ should be the result of some structural dierence of the top layer of the polymer brush (vicinal to the bilayer).

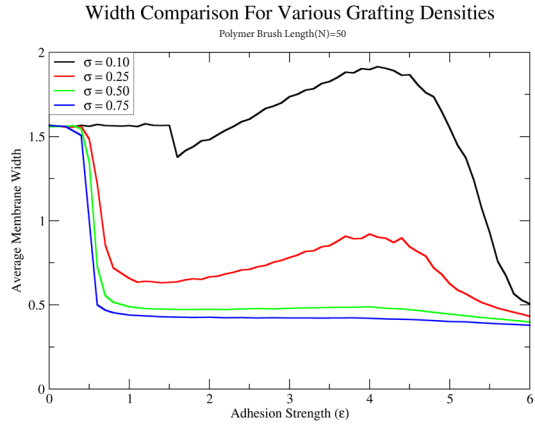

Figure 3. There is a systematic relationship between the width of w and the grafting density of the polymer brush, σ. For increasing σ, the membrane becomes more rigid and the membrane absorbs earlier for more dense systems. Surprisingly, for low density systems, the bilayer has more fluctuations than a free membrane. The non-monotonic behavior becomes less pronounced as σ is increased. This data was collected with $N = 50$.

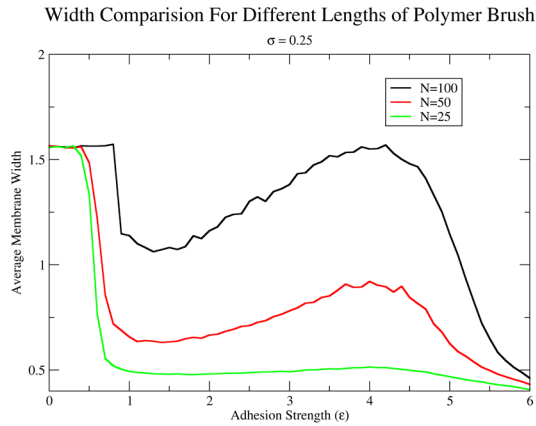

Figure 4. There is a systematic relationship between w and the number of monomers per polymer chain, N. For decreasing N, the membrane becomes more rigid and the membrane absorbs earlier for shorter systems.

The structure factor of a free membrane is given by,

$$S(q) = \frac{k_B T}{\gamma q^2 + \kappa q^4 + \cdots} \tag{8}$$

where γ is the tension coefficient and κ is the bending modulus of the membrane. We can use this structure factor to further investigate how the membrane changes when absorbed onto a polymer brush. Transforming the structure factor to $1/q^2 S(q)$ vs. q^2 allows us to see the contributions of each term in the denominator. Figure 5 shows that for small wavevectors, $1/q^2 S(q)$ actually intercepts the y-axis at a finite value, which increases with increasing $\mathcal{E}$. This is expected as the absorption of the bilayer on the polymer brush leads to an energy cost resulting from vertical translation of the bilayer.

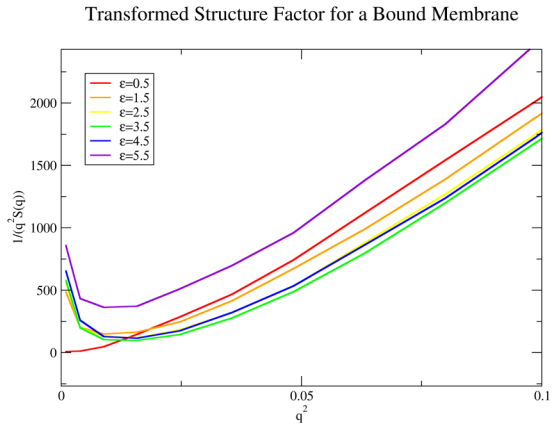

Figure 5. A plot of $1 / q^2 S(q)$ vs. q^2 transformed from Eq.(8) Note that for an unbound membrane ($\mathcal{E} = 0.5$) the plot converges to zero as expected in the case of a tensionless membrane. However, when the bilayer is adsorbed on the brush, $1 / q^2 S(q)$ increases rapidly as $q \to 0$. This indicates that due to binding, the bilayer has a preferred position along the z-axis, leading to the emergence of a mass term in the effective Hamiltonian of the bilayer. Interestingly, for small q (long wavelengths), $1 / q^2 S(q)$ has a non-monotonic behavior, namely it decreases with increasing $\mathcal{E}$, then increases. This behavior mirrors that of w shown above.

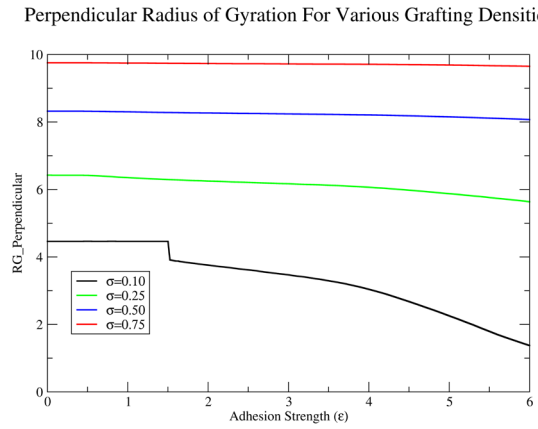

Figure 6. $R_\perp$ monotonously decreases with increasing $\mathcal{E}$. This is expected since the monomers which are within the adhesion sublayer below the bilayer only weakly contribute to $R_\perp$, and the bilayer gets closer to the substrate as $\mathcal{E}$ increases (hence $R_\perp$ decreases with increasing $\mathcal{E}$). This is to say that the behavior of $R_\perp$ is not surprising and not that interesting (in the sense that it does not help in understanding the non-monotonic behavior of w vs. $\mathcal{E}$).

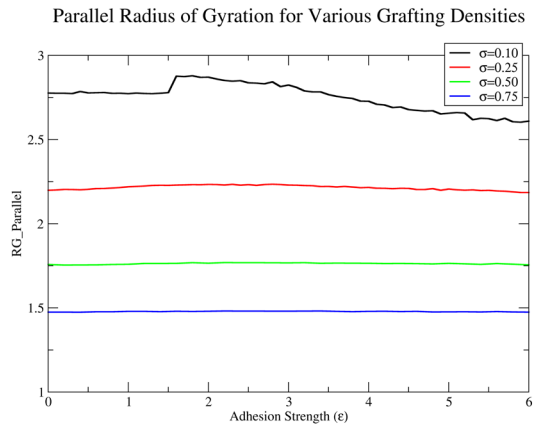

Figure 7. The radius of gyration acquired by summing the radius of gyration along both the x and y axes in quadrature. While the effect is small, there is a non-monotonic trend here that peaks around $\mathcal{E} = 2$. This is due to the binding of the top monomers to the membrane.

In order to understand the non-monotonic behavior of w vs. $\mathcal{E}$, we observed the radius of gyration along the $z-$axis ($R_{\perp}$) and the $xy-$plane ($R_{\parallel}$) to provide more information about the structure of the polymer brush. As shown in Fig. 6, $R_{\perp}$ was not useful in analyzing the non-monotonic behavior of interest. In contrast, Fig. 7 shows that $R_{\parallel}$ has a more interesting non-monotonic behavior, though the change is very weak.

Next, we can look at the contact energy, $E_{contact}$ that results from the interaction of monomers with lipid head groups. From Fig. 2, it is expected that $E_{contact}$ will not depend on the length of the polymer chains, N.

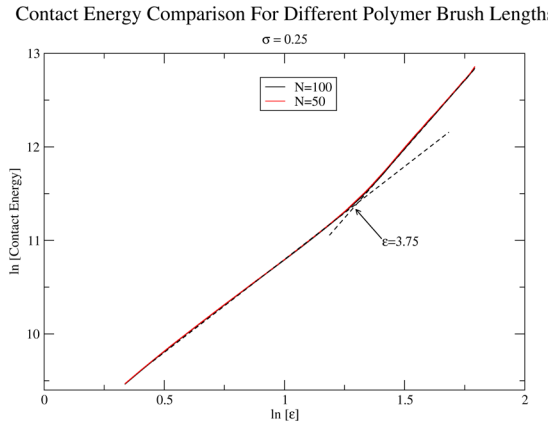

Figure 8. A ln-ln plot of the contact energy between the monomers in the polymer chain and the lipid head groups on the underside of the membrane. $N = 25$ and $N = 50$ chain lengths were used. The contact energy plots lay over top one another, showing that the lower levels of the polymer brush do not participate in the interaction with the membrane. E_{contact} steadily increases with $\mathcal{E}$. However, this increase becomes more pronounced for $\mathcal{E}$ larger than 3.75. This corresponds closely to the peak seen in Figs. 3 and 4.

Figure 8 implies that the non-monotonic behavior of the fluctuations of the membrane is the result of different structural modes of the polymer brush. For low values of the interaction strength between the polymer monomers and the bilayer, the free energy of the system is dominated by the conformational entropy of the portion of the polymer in the vicinity of the bilayer rather than by interactions. The reverse occurs for high values of $\mathcal{E}$. The polymers conformational entropy is higher for low grafting densities than large ones. Hence, the effect above is expected to be stronger for low

values of σ. The non-monotonic behavior of w is indeed more pronounced for low values of σ, as shown in Fig 3.

Conclusions

Overall findings show clear mutual interactions between the lipid membrane and polymer brush. These effects vary with adhesion strength.

For intermediate adhesion strength ($\mathcal{E} \lessapprox 4$), membrane fluctuations increase with adhesion strength. This trend is dominated by the polymer's conformational entropy. This effect is increased with increasing polymer length or decreasing grafting density.

For large adhesion strength ($\mathcal{E} \lessapprox 4$), the membrane fluctuations decrease with increasing adhesion strength. In this region the trend is dominated by the adhesion interaction between the membrane and the polymers.

The fluctuations of the membrane are reduced by either increasing the grafting density or decreasing the length of the polymer brush.

The greatest change in the polymer brush occurs near the membrane. The polymer brush becomes denser directly beneath the membrane as more monomers bind to it. This is evident in the peak occurring in the density profile near the membrane, the small change in the parallel radius of gyration, and the contact energy's independence of brush length. When supported by a polymer brush, the properties of lipid membranes change observably

Because of the clear changes in both the properties of the polymer brush and the lipid membrane, a slightly different model may be presented in the future to help preserve the properties of the lipid membrane in the presence of the brush. All the data here is presented with the assumption that the membrane was tensionless before its adhesion on the membrane. If this assumption is found to be false, the new model will need to change, so the membrane is tensionless in the beginning.

The theoretical understanding acquired from this study is meant to be a launching pad for future experimental work. Using the computational model described here, researchers can learn how their membranes will change if they use a polymer brush support without spending money and time producing the actual polymer brush. If the theoretical results match the desired conditions, an experiment can be conducted with more confidence.

References

Andersson, J., & Köper, I. (2016). Tethered and Polymer Supported Bilayer Lipid Membranes: Structure and Function. *Membranes*, *6*(2), 30. doi: 10.3390/membranes6020030

Deverall, M., Gindl, E., Sinner, E.-K., Besir, H., Ruehe, J., Saxton, M., & Naumann, C. (2005). Membrane Lateral Mobility Obstructed by Polymer-Tethered Lipids Studied at the Single Molecule Level. *Biophysical Journal*, *88*(3), 1875–1886. doi: 10.1529/biophysj.104.050559

Grest, G. S., & Kremer, K. (1986). Molecular dynamics simulation for polymers in the presence of a heat bath. *Physical Review A*, *33*(5), 3628–3631. doi: 10.1103/physreva.33.3628

Laradji, M., & Kumar, P. B. S. (2016). Preface for the special issue "Biomembranes." *International Journal of Advances in Engineering Sciences and Applied Mathematics*, *8*(2), 87–87. doi: 10.1007/s12572-016-0167-0

Mccabe, I. P., & Forstner, M. B. (2013). Polymer Supported Lipid Bilayers. *Open Journal of Biophysics*, *03*(01), 59–69. doi: 10.4236/ojbiphy.2013.31a008

Revalee, J. D., Laradji, M., & Kumar, P. B. S. (2008). Implicit-solvent mesoscale model based on soft-core potentials for self-assembled lipid membranes. *The Journal of Chemical Physics*, *128*(3), 035102. doi: 10.1063/1.2825300